Available online at www.sciencedirect.com
ScienceDirect
Geochimica et Cosmochimica Acta 70 (2006) 4874–4888
Geochimica
www.elsevier.com/locate/gca

Oxidation of arsenopyrite and deposition of gold on the oxidized surfaces: A scanning probe microscopy, tunneling spectroscopy and XPS study

Yuri L. Mikhlin [a,*], Alexander S. Romanchenko [a], Igor P. Asanov [b]

[a] *Institute of Chemistry and Chemical Technology SB RAS, K. Marx str., 42, Krasnoyarsk 660049, Russia*
[b] *Institute of Inorganic Chemistry SB RAS, pr. Lavrent'eva, 3, Novosibirsk 630090, Russia*

Received 21 June 2006; accepted in revised form 20 July 2006

Abstract

We have used ex situ atomic force microscopy (AFM), scanning tunneling microscopy and spectroscopy (STM/STS) and X-ray photoelectron spectroscopy (XPS) to study the surfaces of natural arsenopyrite samples that were electrochemically polarized in 1 M HCl, or leached in acidic solutions containing ferric iron salts, and then reacted with aqueous gold (III) chloride at ambient temperatures. For arsenopyrite oxidized on a positive-going potential sweep, progressively increasing amounts of surface Fe(III)–O and As–O species, and of S/Fe and S/As ratios in a non-stoichiometric sulfidic layer were found. The products formed in the sweep to a potential of 0.6 V (Ag/AgCl) of the passivity region are shaped in about 100 nm protrusions of two sorts, which are arranged in micrometer-size separate areas, while they are largely mixed at higher, "transpassive" potentials. The quantities of surface alteration substances notably decrease after leaching in ferric chloride and ferric sulfate acidic solutions. Passivation of arsenopyrite was suggested to associate with the disordered, metal-deficient surface layer having moderate excess of sulfur rather than with the products of arsenopyrite oxidation. Exposure of arsenopyrite to 10^{-5}–10^{-3} M $AuCl_4^-$ (pH 2) solutions results in the deposition of 8–50 nm gold particles; only a small fraction of the gold is present as Au(I)–S species. The electrochemical oxidation at 0.6 V or ageing of arsenopyrite in air promotes the subsequent gold deposition; in contrast, the amount of Au deposited on arsenopyrite that was treated by leaching in ferric chloride and sulfate solutions was about 10 times smaller than with polished arsenopyrite samples. It has been concluded that reducing agents formed as intermediates of arsenopyrite decomposition facilitate the Au^0 cementation although other factors related to the surface state of the arsenopyrite play a role as well. A decrease in the tunneling current magnitudes with decreasing the Au^0 particle size has been revealed using STS. This effect along with the increase by 0.2–0.5 eV in the XPS Au 4f binding energies were tentatively ascribed to retarding the electron transitions by emerging electrostatic charge on gold nanoparticles (Coulomb blockade). Possible mechanisms for the effects, and their potential role in the deposition and hydrometallurgy of "invisible" gold are discussed.

1. Introduction

Arsenopyrite, FeAsS, is the most abundant mineral of arsenic and a common constituent of Au-bearing sulfide ores. It has a structure based on that of marcasite, FeS_2, with $(As–S)^{2-}$ units instead of disulfide anions (Tossell et al., 1981). Surface reactions of FeAsS play an important role both in the formation of gold deposits and the recovery of Au; also, As, Fe, and S released during oxidation of arsenopyrite are of serious environmental concern (Paktunc et al., 2003; Yunmei et al., 2004). The mechanisms of relevant reactions are still insufficiently understood, particularly because the processes in aqueous media, usually electrochemical in nature, are deeply complicated by semiconducting properties of sulfide minerals, so the interfacial transfer of electrons and the transport of charge carriers between different sites at which the various reactions occur are critically dependent upon the precise composition and local characteristics of the appropriate spatial regions

* Corresponding author.
E-mail address: yumikh@icct.ru (Y.L. Mikhlin).

0016-7037/$ - see front matter © 2006 Elsevier Inc. All rights reserved.
doi:10.1016/j.gca.2006.07.021

(Rimstidt and Vaughan, 2003). The electrochemical oxidation of arsenopyrite occurs in two steps associated with passivation at moderate positive potentials and "transpassive" behavior at higher ones (Kostina and Chernyak, 1976; Cruz et al., 1997; Lázaro et al., 1997; Lin and Zheng, 1997; Costa et al., 2002). Lin and Zheng (1997) proposed that the dissolution of arsenopyrite in acidic chloride solutions is retarded by elemental sulfur that is oxidized to sulfate at the second step. However, although the elemental sulfur is the predominant surface product of the electrochemical, bacterial and abiotic ferric iron oxidation of arsenopyrite, it does not seem to form a continuous film and scarcely passivates the mineral surfaces since its removal produces no significant change in the dissolution rate of the underlying mineral (McGuire et al., 2001a,b,c; Costa et al., 2002). Aside from elemental sulfur, thiosulfate, sulfate, various compounds of As in oxidation states up to +5, and Fe(III)–O species were found on arsenopyrite reacted under various conditions by XPS (Buckley and Walker, 1988–1989; Richardson and Vaughan, 1989; Nesbitt et al., 1995; Schaufuss et al., 2000; Costa et al., 2002; Jones et al., 2003; Mikhlin et al., 2003b), Raman spectroscopy (McGuire et al., 2001b,c; Costa et al., 2002), and X-ray absorption spectroscopy (XANES) (Mikhlin and Tomashevich, 2005). Several researchers (Buckley and Walker, 1988–1989; Nesbitt et al., 1995; Costa et al., 2002; Mikhlin et al., 2003a,b) pointed out the formation of non-stoichiometric, S-rich surface layers which were considered responsible for passivity of mineral sulfides (Buckley et al., 1985; Hackl et al., 1995; Mikhlin et al., 2003a, 2004a,b).

Interaction with aqueous gold-bearing solutions also affects mineral surfaces, the state of which in turn influences adsorptive or reductive deposition of Au along with temperature, pressure, and composition of the metal-bearing fluids (Barnes, 1979). Much of the metal is concentrated as "invisible" gold forming submicrometer metallic particles and Au(I) bonded with sulfur (Fleet and Mumin, 1997; Genkin et al., 1998; den Besten et al., 1999; Simon et al., 1999; Tauson, 1999; Cabri et al., 2000; Palenik et al., 2004; Reich et al., 2005). Precipitation proceeds via the electrochemical mechanism involving anodic oxidation of the sulfide mineral and cathodic reduction of gold (Sakharova et al., 1975; Bou et al., 1998; Maddox et al., 1998). Although gold (I) sulfide complexes are believed to be preferential species under hydrothermal conditions (Widler and Seward, 2002), gold chlorides are involved too, and the stable $AuCl_4^-$ complexes were frequently used in the modeling systems. Jean and Bancroft (1985), Hyland and Bancroft (1989), Mycroft et al. (1995), Maddox et al. (1998), Scaini et al. (1997, 1998) conducted detailed laboratory studies of the deposition of gold on several minerals, including arsenopyrite, using XPS, scanning electron microscopy (SEM) and other techniques. In particular, Maddox et al. (1998) found that gold is present on the arsenopyrite surfaces contacted with 10^{-4} M $KAuCl_4$ + 1 M KCl (pH 3) solution for 10 min mainly as metallic particles less than 50 nm in size, as compared with about 300 nm particles deposited on pyrite. XPS also revealed the formation of minor Au(I) species and an effect of the particle size on Au 4f binding energies. It was concluded that the rate-limiting step in the deposition of gold on pyrite is the reduction of Au^{3+} to Au^+, whereas the rate of reduction of gold on arsenopyrite is controlled significantly by the rate of oxidation of arsenopyrite (Maddox et al., 1998). Heasman et al. (2003) have determined using EXAFS, SEM and transmission electron microscopy (TEM) that the diameters of individual gold clusters deposited on green rust, pyrite, and chalcopyrite were between 2.9 and 7.7 nm and they probably formed composite clusters up to 500 nm.

Only a few researchers have used scanning probe microscopy (SPM) and tunneling spectroscopy (STS) to examine the deposition of noble metals on sulfide minerals, and we are not aware of SPM studies performed on arsenopyrite oxidation. Scanning tunneling microscopy (STM) was applied in order to explore the interaction of gold with PbS surfaces (Eggleston and Hochella, 1991, 1993; Becker et al., 1997). It was found that gold islands grew less quickly on preoxidized galena surfaces than on fresh fracture surfaces; tunneling spectra allowed discrimination the metallic gold (having a uniform density of states near the Fermi level) and semiconducting galena. Ag and Au cementation on copper sulfides, $Cu_{2-x}S$, was studied by atomic force microscopy (AFM) in combination with some other methods by Barzyk et al. (2002). They detected different surface products depending on the nature of the noble metal and the solution composition, with silver tending to form mixed copper–silver sulfides and gold occurring as Au_2S, Au_2S_3 and Au^0. Becker et al. (2003) studied the vapor phase adsorption of Ag, Au, and Cu on the (0 0 1) surface of molybdenite; the researchers put the emphasis mainly on surface Ag–S bonding.

We employed ex situ XPS, AFM, and STM/STS techniques in order to investigate more fully the oxidation of arsenopyrite in acidic solutions and the deposition of gold on the fresh and reacted surfaces. The work was carried out with the particular aim of clarifying the way in which reaction products are spatially distributed over the arsenopyrite surfaces and how they influence the spontaneous precipitation of gold. The results of tunneling spectroscopy and photoelectron spectroscopy for the modified surface layers and for gold particles deposited on the various substrates were compared. This allowed us to shed new light on the phenomena of passivation of arsenopyrite and gold deposition and to reveal charging effects on comparatively large Au^0 nanoparticles that would play an important role in the deposition and leaching of "invisible" gold.

2. Experimental

2.1. Materials and sample preparation

Samples of research grade polycrystalline arsenopyrite (without inclusions of foreign phases, pores and other

visible defects) from Sovetskoe, Krasnoyarsk territory, Russia, with a composition of $Fe_{1.0}As_{0.97}S_{0.96}$ and containing Cu 0.175, Si 0.16, Zn 0.094, Ni 0.041 wt% as impurities (determined using X-ray fluorescence analysis), were cut and polished at silicon carbide paper to approximately 5 mm × 4 mm × 3 mm. The polished surfaces were cleaned by wet filter paper to remove fine particles before a chemical or electrochemical treatment. Some specimens were fractured in air just before microscopic studies or conditioning in aqueous solutions; one sample was cleaved with a steel file in the analytical chamber of the XPS instrument under ultra-high vacuum in order to characterize an unoxidized arsenopyrite surface. XPS spectra and AFM images of such surfaces are shown below. For electrochemical experiments, a copper layer was deposited on one sample face, tinned copper wire was soldered to the Cu coating, and then the specimens were embedded in Teflon, with the working face exposed; the electrode without the plastic was employed in XPS experiments. The electrochemical experiments were performed with a potentiostat PI-50-1 equipped with a programmer PR-8 (ZIP, Belarus) in a conventional three-compartment glass cell. Counter and reference electrodes were Pt wire and saturated Ag/AgCl electrode, respectively; all potentials below are given with respect to the latter. The voltammetric experiments were conducted using a stationary electrode at 20 ± 1 °C, the sweep rate usually was 5 mV/s. Arsenopyrite sample was polarized during a sweep going from the rest potential of about 0.3 V to a predetermined potential value and then the sample was immediately extracted, rinsed with distilled water in order to remove remains of the electrolytes, and examined by ex situ XPS and SPM as described below. In leaching experiments, the samples were conditioned in 1 M HCl, 1 M HCl + 0.4 M $FeCl_3$, 0.5 M H_2SO_4 + 0.2 M $Fe_2(SO_4)_3$ or 1 M HNO_3 + 0.4 M $Fe(NO_3)_3$ media without stirring at 50 ± 1 °C, rinsed quickly with a relevant cold dilute acid and then with water. Then they were transferred into a vacuum chamber of the XPS spectrometer, allowed to desiccate in the atmosphere and examined with SPM, or placed into an Au-bearing solution. Gold was deposited on arsenopyrite from unstirred 10^{-5}–10^{-3} M solutions of $HAuCl_4$ adjusted to pH 2 with HCl at 20 ± 1 °C. The reacted samples were rinsed with water before examination. All the solutions were prepared from reagent grade chemicals and doubly distilled water; no attempt was made to prevent ingress of air.

2.2. Instrumentation

AFM, STM and STS investigations were performed using a multimode Solver P47 device (NT-MDT, Russia) equipped with a 14 μm scanner under ambient conditions. Contact mode AFM, both in situ and ex situ, turned out to be poorly sensitive to products of arsenopyrite oxidation and gold nanoparticles. Moreover, in situ techniques were not suitable for prolonged leaching experiments under elevated temperatures, and STS studies in electrolyte solutions were seriously complicated by parasitic faradaic currents. Unfortunately, we did not have access to vacuum AFM or STM/STS installations, and so the specimens described above were generally examined in air, with special attention given to reproducibility of STS data. The AFM experiments were conducted using mainly ex situ tapping mode (TM-AFM), with simultaneous height and phase image recording. No less than three points at each of at least three to four arsenopyrite samples treated in parallel were imaged. Typical force constant of the silicon cantilever was 6 N/m. AFM and STM images were collected at the scan rate of 1–2 Hz with 256 or 512 lines per scan; no smoothing procedure was applied. The tips used in STM/STS measurements were mechanically cut 90% Pt–10% Ir wires. Positive bias was defined as a positive voltage on the sample with respect to the tip. The $I - V$ and $dI/dV - V$ curves were measured using a fixed tip-sample separation by breaking the feedback circuit for a few microseconds at a desired surface location. All curves shown in this article represent the average character of at least 10 reproducible measurements without changing the lateral position, the tip-sample distance and the potential sweep rate. The XPS spectra were acquired in two series of experiments using an X-ray photoelectron spectrometer VG Microtech with Mg Kα X-ray source at room temperature and pressure of $\sim 10^{-8}$ Pa; the analyzer pass energy was 20 eV. Binding energies were corrected for electrostatic charging using the C 1s peak (285.0 eV). A Gaussian–Lorenzian line shape was employed to fit the peaks after subtracting a non-linear Shirley background; the least number of components providing reasonable agreement with the raw data were used. Surface atomic ratios of elements were determined from integrated peak areas corrected for the experimental photoionization cross-sections (Briggs and Seah, 1990). The spectra shown in figures below were normalized in height.

3. Results

3.1. Pristine and air-oxidized arsenopyrite

Fig. 1 shows representative tapping mode AFM images from fracture and polished arsenopyrite samples. The fracture surfaces (Fig. 1a) exhibit no visible oxidation products but rather rough relief due to imperfect arsenopyrite cleavage. Scratches from polishing are observable both in the height and phase images of a polished specimen (Fig. 1b), and less than 100 nm in diameter particles of arsenopyrite debris and oxidation products are better discernible in the phase image.

X-ray photoelectron spectra of arsenopyrite cleaved in vacuum, and of the sample polished in air are presented in Fig. 2. The narrow peak at 707.3 eV in the Fe 2p spectra is due to singlet Fe(II) in arsenopyrite phase, and the intensity above about 709 eV originates from Fe(III)–O species. The broad high-energy maxima consist of at least four multiplet peaks for the Fe(III) ions (for example, Nesbitt et al.,

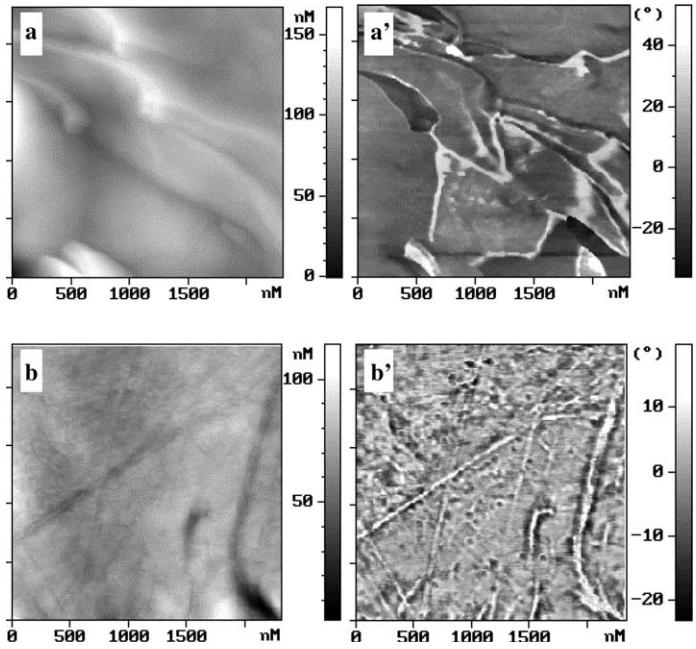

Fig. 1. Typical height (left panels a, b) and phase (a′, b′) TM-AFM images of (a) fractured and (b) polished in air arsenopyrite samples.

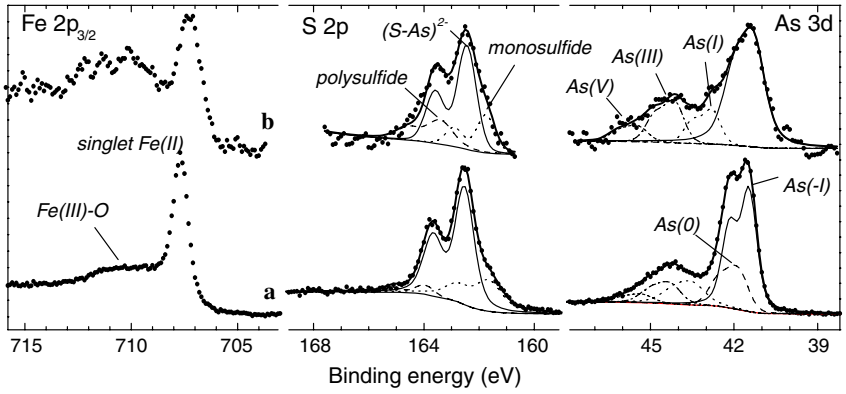

Fig. 2. XPS spectra from arsenopyrite (a) cleaved in vacuum and (b) polished in air. The raw data are depicted as points and the background and the fitting results are given by lines.

1995), and the fitting procedure seems rather arbitrary because of a big number of variable parameters. Consequently, only contributions from singlet ferrous iron and ferric iron were separated in this study (Table 1). The Fe 2p spectrum indicates that the polished surface is noticeably oxidized. This is consistent with As 3d spectra showing, aside from the main As $3d_{5/2,3/2}$ doublet at 41.2 eV, additional contributions at 42.0, 42.8, 44.3, and 45.2 eV, probably from As(0), As(I), As(III), and As(V) species, respectively (Buckley and Walker, 1988–1989; Nesbitt et al., 1995; Costa et al., 2002). Such a fitting, however, seems to be not quite unique due to a large number of overlapping peaks, which may correspond to surface intermediates rather than stable species, so we are careful with ascribing the lines to certain compounds.

The S 2p spectra are better fitted with three doublets, with the largest one at 162.4 eV originating from $(AsS)^{2-}$ anions of arsenopyrite. The peak at 161.4 is due to monosulfide and that at 163.6 eV is usually associated with polysulfide (Buckley and Walker, 1988–1989; Nesbitt et al., 1995); some increase in the intensity of the latter is observed after the polishing. In general, the spectra and their assignments agree with those reported in the literature (Buckley and Walker, 1988–1989; Nesbitt et al., 1995; Schaufuss et al., 2000).

3.2. Arsenopyrite electrochemically polarized in 1 M HCl

The cyclic voltammogram of arsenopyrite in 1 M HCl solution is presented in Fig. 3. The anodic current in the positive-going sweep is small at potentials less than 0.6–0.7 V and rises at more positive potentials. Two weak cathodic maxima at approximately 0.15 and −0.25 V, and a current surge at potentials more negative than −0.3 V are observed

Table 1
XPS surface compositions for arsenopyrite treated under various conditions

FeAsS samples	As		S		Fe		Au		Atomic ratios		
	BE/eV	I/%	BE/eV	I/%	BE/eV	I/%	BE/eV	I/%	S/Fe	S/As	S/Au
Abraded in vacuum	41.5	52	161.6	26	707.7	71	—	—	1.12	0.81	—
	41.9	19	162.5	69	710[a]	29[a]					
	43.5	14	164.0	5							
	44.3	11									
	45.3	4									
Polished in air	41.3	61	161.7	20	707.2	48	—	—	0.88	0.65	—
	42.8	14	162.4	62	710[a]	52[a]					
	44.1	18	163.6	18							
	45.5	7									
Polarized to −0.3 V[b]	41.4	55	161.4	33	707.4	55	—	—	0.96	0.70	—
	42.4	8	162.6	67	710[a]	45[a]					
	44.1	15									
	45.4	22									
Polarized to 0.6 V[b]	41.3	58	161.1	18	707.5	48	—	—	1.39	1.08	—
	42.0	10	162.3	62	710[a]	52[a]					
	43.1	10	163.4	20							
	44.5	16									
	45.3	6									
Polarized to 0.9 V[b]	41.3	51	160.9	14	707.1	44	—	—	2.0	1.06	—
	41.8	4	162.2	70	710[a]	56[a]					
	43.6	13	163.4	16							
	44.5	10									
	45.2	22									
Leached in a $FeCl_3$ solution[c]	40.9	48	161.7	16	707.6	71	—	—	3.33	2.44	—
	41.2	18	162.4	51	710[a]	29[a]					
	42.6	10	163.3	33							
	43.6	15									
	45.2	9									
Leached in a $Fe_2(SO_4)_3$ solution[d]	41.5	47	161.6	13	707.5	64	—	—	1.89	1.33	—
	42.0	25	162.6	60	710[a]	36[a]					
	43.5	7	163.7	19							
	44.1	11	168.6	8							
	45.1	10									
Reacted in 10^{-4} M $HAuCl_4$[e]	41.7	54	161.8	19	707.5	51	84.0	10	2.51	1.87	2.44
	42.3	15	162.7	41	710[a]	49[a]	84.3	84			
	43.7	15	163.5	23			85.3	6			
	44.8	14	165.8	3							
	45.7	2	167.9	6							
			169.1	8							
Leached in $FeCl_3$[c] and reacted with 10^{-4} M $HAuCl_4$[e]	41.7	29	161.7	14	707.5	42	84.0	9	1.55	0.89	22.7
	42.4	10	162.4	45	710[a]	58[a]	84.4	78			
	43.8	17	163.3	24			85.0	23			
	44.7	32	168.0	7							
	45.7	12	168.7	10							
Leached in $Fe_2(SO_4)_3$[d] and reacted with 10^{-4} M $HAuCl_4$[e]	41.7	34	161.6	14	707.7	40	84.4	61	1.84	1.39	46.6
	42.4	12	162.3	30	710[a]	60[a]	85.5	39			
	43.9	15	163.5	19							
	44.7	22	166.1	2							
	45.7	17	168.7	35							

[a] Approximate values for Fe(III)–O species.
[b] Polarization in the potential sweep, 1 M HCl, 5 mV/s, 20 °C (see text).
[c,d] Leaching in 1 M HCl + 0.4 M $FeCl_3$ and 0.5 M H_2SO_4 + 0.2 M $Fe_2(SO_4)_3$, respectively, at 50 °C for 1 h.
[e] Solution of 10^{-4} M $HAuCl_4$ (pH 2) for 5 min 20 °C.

on the negative-going sweep; the charge associated with the reduction is much less than that passed in the electrooxidation processes. Similar data have previously been acquired at different arsenopyrite electrodes (Kostina and Chernyak, 1976; Cruz et al., 1997; Lázaro et al., 1997; Lin and Zheng, 1997; Costa et al., 2002); they are consistent with the idea

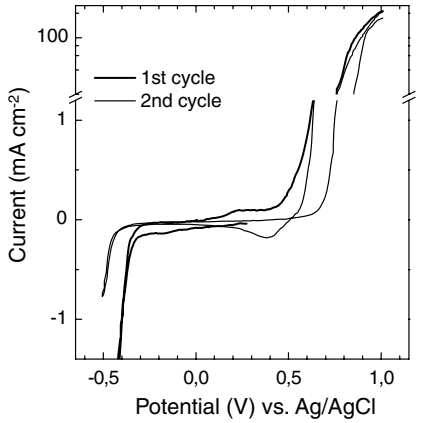

Fig. 3. Cyclic voltammogram for a stationary arsenopyrite electrode. The sweep was started in the negative-going direction from the rest potential of roughly 0.3 V. 1 M HCl, 5 mV/s, 20 °C.

that a passivating layer decomposes at high enough overpotentials, thereby accelerating the oxidation of underlying mineral. In the second cycle, the surges of cathodic and anodic currents are shifted to more negative and more positive potentials, respectively, extending the passivity region; the cathodic maximum arising at about +0.4 V is due to the reduction of Fe(III) species. Other small features on the voltammetric curves may be rationalized largely in terms of transformations occurring within the disordered metal-deficient surface layer (Mikhlin et al., 2001, 2003a,b, 2004a,b; see also Section 4). The voltammograms obtained in hydrochloric, sulfuric and nitric acid media are similar but the current magnitudes, both anodic and cathodic, are less in the sulfuric acid solution (Mikhlin et al., 2003a).

Fig. 4a shows height and phase TM-AFM images of arsenopyrite polarized in 1 M HCl on the sweep to a potential of 0.6 V. At least two sorts of protrusions having comparable diameters of about 100 nm but different heights are arranged in micrometer-scale areas of irregular shape which are clearly visible in the phase image. This picture remains almost intact after ageing the specimens in the laboratory air for several weeks. As the potential sweep limit extends to higher potentials, the covering becomes denser and more uniform as various substances seem to be largely mixed (Fig. 4b). Products of arsenopyrite decomposition

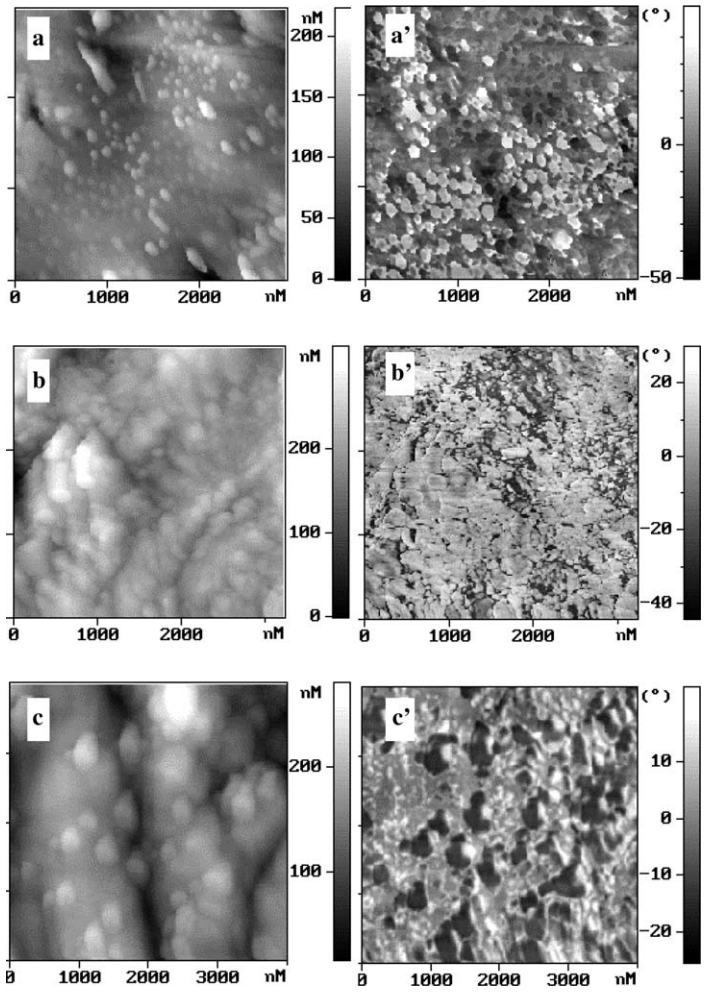

Fig. 4. TM-AFM images (height, left panels, and phase, right panels) of arsenopyrite electrode after the potential sweep to (a) 0.6 V, (b) 0.9 V and (c) −0.3 V. 1 M HCl, 5 mV/s, 20 °C.

are well differentiated in the AFM images from the electrode polarized in a negative-going sweep (Fig. 4c). Larger islands reach about 500 nm in size and 100 nm in height, whereas the smaller ones are only 1–3 nm high and are discernible mainly as whitish spots in the phase image.

XPS analysis (Fig. 5) revealed increasing quantities of the oxidized As and Fe surface species after the positive-going potential sweep. As(III)–O (BE of about 44.3 eV) prevails among arsenic products after arsenopyrite has been oxidized in the sweep to 0.6 V, and the amount of As(V)–O species increase with extending the positive-going scan to 0.9 V. The S 2p spectra show minimal responses from S–O species at BE higher than 165 eV. The lines of underlying arsenopyrite still notably contribute to the spectra, almost certainly due to the evaporative loss of elemental sulfur into the ultra-high vacuum at room temperature (Buckley and Woods, 1984; Kartio et al., 1997), indicating the depletion of a reacted surface layer of arsenopyrite in Fe and As (Table 1).

Cathodic treatment of a fresh surface of the arsenopyrite electrode in the sweep to −0.3 V entails an unexpected increase in the proportion of As(V) species, whereas the high-energy "polysulfide" component in the S 2p spectrum disappears and the intensity of monosulfide rises. The atomic S/As and S/Fe ratios (Table 1) suggest some deficiency of sulfur in the surface layer as compared with polished and oxidized surfaces. These findings imply that the electrochemical reduction of arsenopyrite involves breakage of As–S (and minor S–S) bonds, releasing sulfur as H_2S followed by rapid chemical oxidation of Fe and As

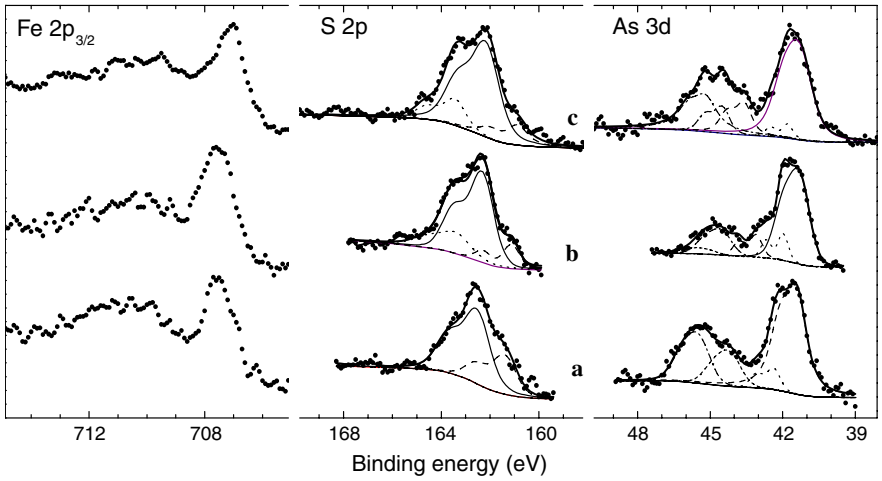

Fig. 5. XPS spectra from arsenopyrite electrode after the potential sweep to (a) −0.3 V, (b) 0.6 V, and (c) 0.9 V initiated from the rest potential of 0.3 V. 1 M HCl, 5 mV/s, 20 °C.

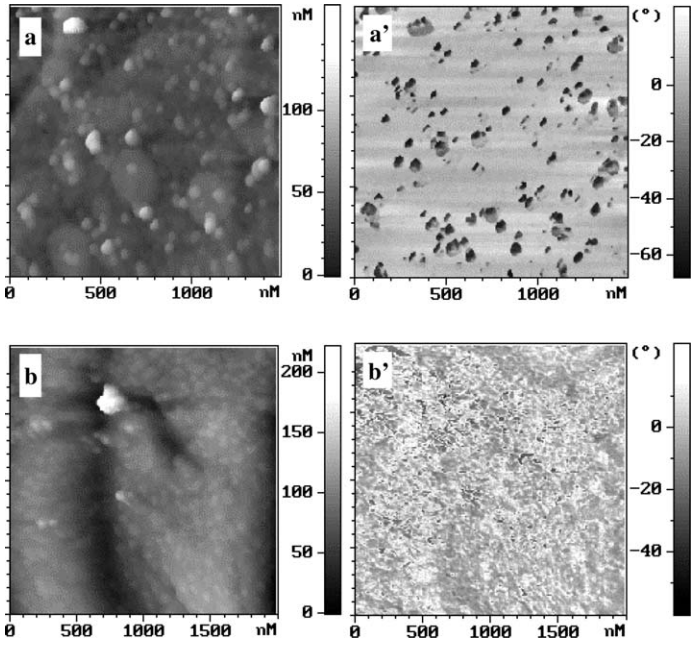

Fig. 6. AFM images (a, b–height, a′, b′–phase) of arsenopyrite samples leached at 50 °C in (a) 1 M HCl + 0.4 M $FeCl_3$ for 1 h; (b) 0.5 M H_2SO_4 + 0.2 M $Fe_2(SO_4)_3$ for 1 h.

intermediates on the reduced surface. This conforms to the observation that electrochemically reduced surfaces of metal sulfides oxidize faster than polished or fractured surfaces (see, for example, for chalcopyrite Cattarin et al., 1990; Mikhlin et al., 2004b). In general, association of substances detected by XPS with those observed by SPM is ambiguous, first of all due to the loss of elemental sulfur, the main surface product of arsenopyrite oxidation (Cruz et al., 1997; McGuire et al., 2001a,c), into the spectrometer chamber vacuum. The cathodic polarization does not produce the sulfur, so the AFM (Fig. 4c) appears to show the growth of protrusions composed of ferric arsenite- and arsenate-like compounds.

3.3. Surfaces oxidized in acidic ferric iron solutions

The leaching in ferric sulfate or ferric chloride solutions for a few minutes produces etch pits of 10–30 nm in diameter and spherical globules less than 100 nm in size (electronic annex, EA-1-1,2). Then the pits disappear and an array of globules about 50–100 nm diameter develop together with a small number of greater, up to 500 nm particles (Fig. 6a and b). For FeAsS treated with the ferric sulfate solution for 1 h, less than 10 nm high protrusions with irregular shape cover a considerable share of the arsenopyrite surface (Fig. 6b).

The photoelectron spectra (Fig. 7) also demonstrate noticeably less quantities of oxidized As and Fe species on the leached surfaces than on the surfaces treated electrochemically, whereas the proportion of polysulfide and the surface depletion in As and Fe are greater, especially in the case of ferric chloride solution. The formation of realgar, As_4S_4, which would exhibit an As 3d peak at 43.1–43.4 eV and S 2p peak at 162.8–163.1 eV (Pratt and Nesbitt, 2000; Bullen et al., 2003), or orpiment, As_2S_3, having the relevant BE of 43.4–43.8 and 162.5–162.7 eV, respectively (Costa et al., 2002; Gheorghiu-de La Rocque et al., 2002), should not be ruled out but seems unlikely (Mikhlin and Tomashevich, 2005). It is worth noting that only 1 min exposure to a ferric nitrate solution results in the surface entirely coated with products (EA-1-3), which mainly consist of Fe(III), As(V), and oxysulfur anions with S atoms in the oxidation states from +2 to +6, according to AFM, XPS, FTIR (not shown in figures) and XANES data (Mikhlin and Tomashevich, 2005).

3.4. Gold deposition on arsenopyrite

The uptake of gold by arsenopyrite was estimated using STM and AFM and it was quantitatively determined from XPS analysis, within the uncertainties inherent to the method. All these techniques show that gold precipitation increases with increasing concentration of gold solutions and contact time under identical conditions. The precipitation is, therefore, kinetically controlled, but relative rates rather than their precise values can be obtained on the basis of the available data. STM shows that Au^0 particles deposited on fracture or polished surfaces from a 10^{-4} M $AuCl_4^-$ solution have diameters mainly in the range 5–30 nm (Fig. 8a and b). A coating composed of approximately 10 nm gold particles cover considerable part of the surface of arsenopyrite reacted for 10 min; more prolonged deposition creates a number of 50–100 nm gold islands on top of the first Au layer (EA-1-4). The precipitation of gold is somewhat faster if arsenopyrite was polished in air or a fractured arsenopyrite plate was preliminary exposed to atmosphere for several days. The quantities of Au^0 decrease for arsenopyrite polarized cathodically or etched in a non-oxidative hydrochloric acid solution before the deposition. A continuous film formed by 10–15 nm gold particles was observed in the case of arsenopyrite oxidized in the potential sweep to a potential of 0.6 V in 1 M HCl and then reacted in the 10^{-4} M $AuCl_4^-$ solution (not shown in figures). However, only a small number of 10–30 nm Au^0 particles were found for the mineral previously anodized in the sweep to 0.9 V (Fig. 8c).

The leaching in Fe^{3+}-containing media inhibits subsequent deposition of gold. AFM showed a larger number of spherical particles, including the globules of approximately 500 nm in diameter (EA-1-5,6) composed possibly of ferric iron sulfate (see XPS data below), but gold particles were not identified definitely. STM detected no large particles due to their non-conducting nature and revealed small amount of 10–50 nm gold particles on a patterned arsenopyrite surface (Fig. 8d).

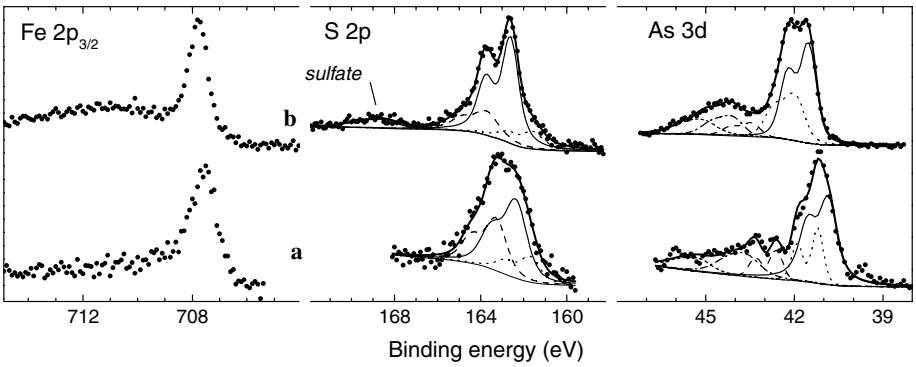

Fig. 7. XPS spectra from arsenopyrite leached in (a) 1 M HCl + 0.4 M $FeCl_3$ and (b) 0.5 M H_2SO_4 + 0.2 M $Fe_2(SO_4)_3$ solutions at 50 °C for 1 h.

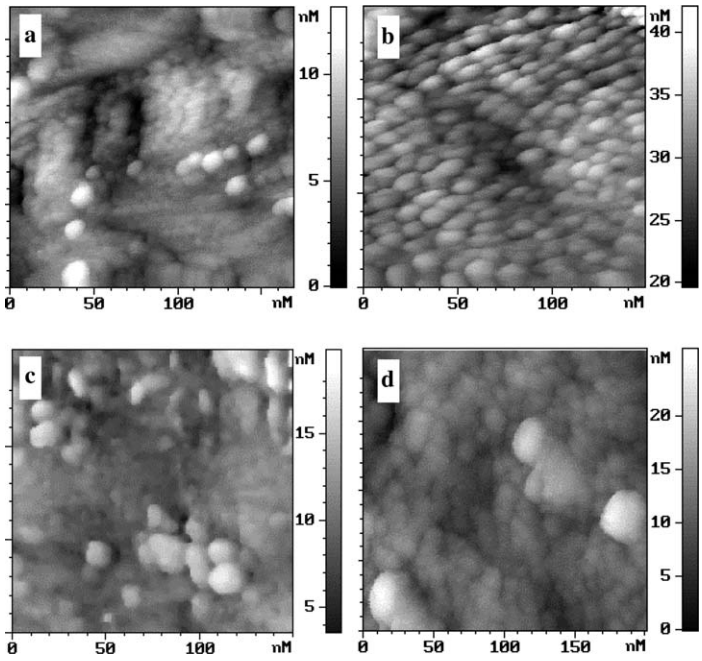

Fig. 8. STM images ($I_{SP} = 0.5$ nA, $V_B = 0.1$ V) of the surfaces of polished arsenopyrite reacted in 10^{-4} M $HAuCl_4$ (pH 2) for (a) 2 min and (b), (c), (d) 10 min. Arsenopyrite was oxidized in (c) 1 M HCl on the positive-going scan to 0.9 V, and (d) 1 M HCl + 0.4 M $FeCl_3$ (50 °C, 1 h) before the gold deposition.

The Fe, As and S photoelectron spectra of arsenopyrite polished and then treated with aqueous $AuCl_4^-$ resemble those for the mineral leached in the ferric salt solutions, including the depletion of the sulfide phase in Fe and As (Table 1). The amounts of oxidized As, Fe and S species, especially As(III) and sulfate, further increase for the samples preoxidized in the Fe^{3+}-containing media before the gold deposition. The relative intensities of Au 4f spectra are more than 10 times lower for such specimens as compared with the deposition on fresh surfaces, in accord with the SPM data. The Au $4f_{7/2}$ lines are better fitted with three peaks at 84.0, 84.2–84.5 eV (most intensive) and about 85.3 eV, which are thought to represent bulk Au^0, small Au^0 nanoparticles or/and surface gold atoms, and Au(I)–S species, respectively (Mycroft et al., 1995; Maddox et al., 1998). A share of Au(I) is minor, but it increases with diminishing the total amount of precipitated gold. An increase in the binding energies of metallic gold with decreasing particle size (see also Mycroft et al., 1995; Maddox et al., 1998 and reference herein) appears to be a consequence of a temporal charging of the nanoparticle due to the photoionization process, lessening kinetic energies of the photoelectrons by interaction with holes formed on the Au nanoparticles in final state (Hövel et al., 1998; Ohgi and Fujita, 2003; Boyen et al., 2005). However, the dimension of the gold clusters supported on other substrates was commonly less than 5 nm, while the Au particles on arsenopyrite are notably larger.

Fig. 10 shows selected STS current–voltage plots from initial and reacted arsenopyrite specimens. The tunneling spectra measured on fresh fracture surfaces are rather symmetric and display a conductance gap of approximately 1 eV, which seems to be close to the band gap width of bulk arsenopyrite and pyrite (0.95 eV after Eyert et al., 1998). For the sample electrochemically oxidized on the sweep to potentials less than about 0.7 V (lying in the passivity region), the tunneling current rises more rapidly at negative biases, indicating a band gap narrowing. The spectra from the samples oxidized on the sweep to higher, ''transpassive'' potentials and those leached in the Fe^{3+} solutions are usually characterized by decreased tunneling currents at positive biases. It is worth to mention here that the spectra were acquired ex situ, after the electrochemical polarization has been terminated, and so the Fermi level has moved away from the valence band into new stationary positions at the surface. Furthermore, as the near-surface layer has became sulfur-enriched and disordered, the I–V curves were actually measured at materials that are distinct from initial arsenopyrite and have modified electronic band structures (Mikhlin and Tomashevich, 2005; EA-1-7) or/and comprise plentiful specific defects generated by the oxidation.

Tunneling spectra measured above gold particles depend upon their size. The I–V plots (Fig. 10b, 1 and 2) illustrate a positive correlation between the current magnitude and the diameter of Au particles, and the relevant dI/dV curves (not in figures) have clear minimum near the bias offset. These findings could be explained in terms of Coulomb blockade effects typical for ultrafine gold particles (Ohgi and Fujita, 2003; Daniel and Astruc, 2004 and references herein), when arising electric charge of a particle retards electron transfer in a junction with a very small capacitance. The physics underlying the charging effects is similar in photoelectron spectroscopy and tunneling spectroscopy, so the high-energy shifts of XPS Au 4f lines and the

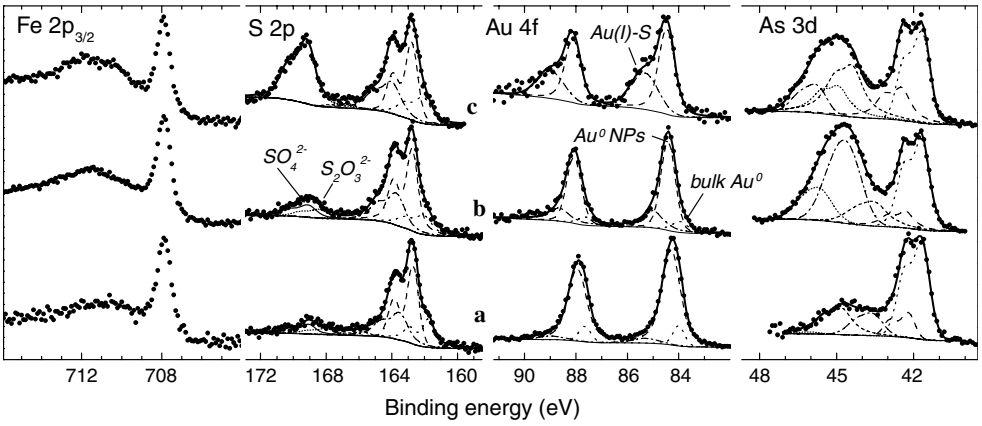

Fig. 9. XPS spectra of arsenopyrite reacted with a 10^{-4} M $HAuCl_4$ solution for 5 min: samples (a) polished and leached in (b) 1 M HCl + 0.4 M $FeCl_3$ and (c) 0.5 M H_2SO_4 + 0.2 M $Fe_2(SO_4)_3$ solutions (50 °C, 1 h) before the gold deposition.

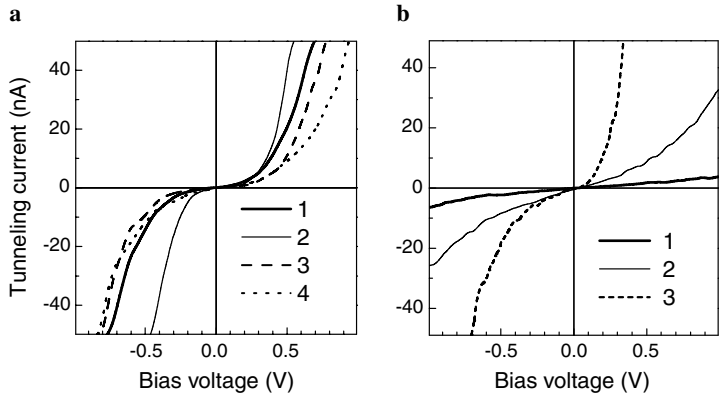

Fig. 10. Typical tunneling spectra measured (a) above arsenopyrite: (1) air-fractured surface, specimens electrochemically oxidized in 1 M HCl on the potential scan to (2) 0.6 V and (3) 0.9 V (5 mV/s, 20 °C), or (4) reacted in 1 M HCl + 0.4 M $FeCl_3$ media at 50 °C for 1 h (AFM images of such surfaces are given in Figs. 1a, 4a and b, and 6a, respectively); (b) above separate gold nanoparticles of about (1) 10 nm and (2) 30 nm diameter, and (3) a solid film composed of about 10 nm Au particles deposited on polished arsenopyrite surfaces (see text for more detail).

suppression of tunneling currents in STS appear to have the same origin. We observed the ''Coulomb blockade''-type curves both on isolated particles less than 50 nm in size and quasi-continuous coatings composed of 10 nm or less Au particles. The *I–V* plots acquired over the gold films or sponges formed due to a large Au uptake were characteristic of a bulk metal. In some cases, STS suggests a rectifying Schottky barrier (i.e., metal–semiconductor interface) rather than Coulomb blockade. Such tunneling spectra are usual for silver precipitated on arsenopyrite and are probably due to the formation of the metal sulfide underlayer; these data will be published in detail elsewhere.

4. Discussion

4.1. Reactivity and passivation of arsenopyrite

The decomposition of arsenopyrite proceeds via breaking Fe–As, Fe–S, and As–S bonds both under oxidative and reductive conditions. At positive potentials, As and Fe ions are released from the solid leaving a sulfur-rich surface, and monosulfide species combine to form polysulfide anions. The electrochemical oxidation of arsenopyrite can be described as involving conventional reactions

$$\mathrm{FeAsS} + 3\mathrm{H_2O} \rightarrow a\mathrm{Fe^{2+}} + b\mathrm{H_2AsO_3^-} + \mathrm{Fe_{1-a}As_{1-b}S_{1-c}} + 0.5c(\mathrm{S^0} + \mathrm{HSO_4^-}) + (6 - 2b - 0.5c)\mathrm{H^+} + (6 + 2a - 3b)\mathrm{e} \quad (1)$$

$$\mathrm{FeAsS} + 4\mathrm{H_2O} \rightarrow x\mathrm{Fe^{3+}} + y\mathrm{H_2AsO_4^-} + \mathrm{Fe_{1-x}As_{1-y}S_{1-z}} + z(\mathrm{S_0} + \mathrm{HSO_4^-}) + (8 - 2y - z)\mathrm{H^+} + (8 + 3x - 3y)e \quad (2)$$

which reflect a varying enrichment of the reacted arsenopyrite surfaces in sulfur ($c < a, b$; $z < x, y$; and $a, b < x, y$), and variable yields of Fe(III), As(III) and As(V) species. Sulfur is released at a slower rate forming elemental sulfur and sulfate (McGuire et al., 2001a,c), but surface concentrations of oxysulfur species are usually rather small. There is probably no sharp boundary between the stages as the composition and properties of the surface layers seem altering gradually with increasing potential, in conformity with the almost featureless anodic curves (Fig. 3). The differences in the reactivity of arsenopyrite in chloride and sulfate

electrolytes appear to be due to the influence of anions on the rates of the iron and, possibly, arsenic release from arsenopyrite, and the oxidative ability of the Fe^{3+}/Fe^{2+} couple over the oxidative leaching.

Surface substances could cause passivation by inhibiting the passage of reactants to, or solubilized reaction products from, the underlying sulfide phase. However, the SPM and XPS results suggest that the solid products play an insignificant role in passivation of arsenopyrite. In particular, neither elemental sulfur nor As and Fe compounds form an uncompromised coating on the surfaces oxidized electrochemically at potentials of passivation, while a film of this sort seems to appear at more positive, "transpassive" potentials. The rates of arsenopyrite leaching in ferric iron salt solutions increases in the order $Fe_2(SO_4)_3 < FeCl_3 < Fe(NO_3)_3$, while the quantity of the surface products changes in the range $FeCl_3 < Fe_2(SO_4)_3 \ll Fe(NO_3)_3$. McGuire et al. (2001a) have arrived at analogous conclusion as they found using Raman microscopy that elemental sulfur appeared on arsenopyrite and pyrite surfaces that had been oxidized in ferric iron solutions as isolated patches on the order of tens of micrometers in size and did not form a continuous passivating layer. It is important to note that we have found the spatially heterogeneous distribution of the products both in nanometer and micrometer scales (Fig. 4a). Although the inherent inhomogeneity of a mineral may give rise to active sites on the surface, blocking of which by small amounts of products or adsorbates would significantly influence the average rates of chemical processes, there is no evidence of such a passivation mechanism for arsenopyrite dissolution.

It was previously proposed (Mikhlin et al., 2001, 2002, 2003a,b, 2004a,b) that the passivity of metal sulfides is connected with the non-stoichiometric disordered surface layer having comparably low metal deficiency. Such a layer contains positive donor-like centers D^+ in rather rigid, inelastic structural environment, which arises as a result of holes trapped at orbitals of atoms that constitute the upper portion of the valence band and are most readily oxidized. If these defects distributed at random become widespread, they give rise to large potential fluctuations in the solid and so called Anderson localization of electronic states, sharply decreasing the carriers' mobility and thus the conductivity of the surface layer akin to disordered chalcogenide semiconductors (Mott and Davis, 1979; Tsendin, 1996). Since the upper valence band of reacted arsenopyrite is constructed by Fe 3d orbitals, the defects are likely related with Fe(III) bonded to As and S.

XPS data confirm the formation of the non-stoichiometric surface layer, and the tunneling spectra indicate modified electric properties of the surfaces, giving more credence to the aforementioned model. The local conductance between the tip and the sample becomes even greater after oxidation but this does not contradict the model since the lateral carriers' mobility and the conductivity averaged over the layer are expected to be suppressed as a result of multiple capturing of the charge carriers by the localized states. On the other hand, it was found that the quantities of Fe(III)–O species increased on the passive surfaces of pyrrhotite, implying that these species either cause passivation or, more likely, arise as a consequence of the passivation (Mikhlin et al., 2001, 2002). Electrons may tunnel via a thin dielectric passivating film that retards the transfer of ions or the probe may break the film mechanically (such an impact certainly occurs on surfaces covered by the abundant products which are not seen in STM). Therefore, although the metal-deficient layer almost certainly plays a role, the nature of passivation is not yet conclusively established.

4.2. Reactions of gold deposition

It is commonly accepted that the deposition of gold proceeds via the electrochemical mechanism (Sakharova et al., 1975; Bou et al., 1998; Maddox et al., 1998). Maddox et al. (1998) pointed out that the open-circuit potentials of arsenopyrite and pyrite are mixed potentials, resulting from a balance of oxidation of mineral sulfide and reduction of gold. The authors found that the potential for deposition of gold on pyrite from $AuCl_4^-$ solutions is close to the potential for deposition of gold on gold, whereas the potential for deposition of gold on arsenopyrite is obviously less positive. They concluded that the rate of deposition of gold on pyrite is controlled almost entirely by the rate of reduction of Au(III), and the process on arsenopyrite is controlled significantly by the rate of oxidation of the mineral. However, the corrosion potential lies closer to the one for the faster process (Kiss, 1988), so quite opposite deductions should be made. The open-circuit potential value of 0.3–0.4 V close to that reported by Maddox and co-workers (1998) was observed in the current research, and we believe that the reduction of Au species is slow, while the anodic oxidation of the mineral is relatively rapid. The well-established faster oxidation of arsenopyrite than pyrite also corroborates this conclusion.

The cathodic reactions of gold complexes and the deposition process as a whole depend on the state of the substrate. The surfaces promoting Au deposition are characterized by comparably low excess of sulfur in the reacted sulfide layer and rather high quantities of surface products. The products may be responsible for local redox interaction between gold species and active reducing agents, for example via arbitrary reactions

$$11AuCl_4^- + 3(AsS)^{2-} + 21H_2O \rightarrow 11Au^0 + 3H_2AsO_3^- + 3HSO_4^- + 33H^+ + 44Cl^- \quad (3)$$

$$2AuCl_4^- + 3H_2AsO_3^- + 3H_2O \rightarrow 2Au^0 + 3H_2AsO_4^- + 6H^+ + 8Cl^- \quad (4)$$

$$AuCl_4^- + 3Fe^{2+} + 6H_2O \rightarrow Au^0 + 3FeOOH + 9H^+ + 4Cl^- \quad (5)$$

Recently, Heasman et al. (2003) and O'Loughlin et al. (2003) have demonstrated experimentally that mixed Fe(II)/Fe(III) hydroxides (green rust) are involved in the reduction of aqueous gold complexes. The increase in surface concentrations is larger for oxidized arsenic species than for Fe and S species (Figs. 2, 5 and 9), suggesting a role of As intermediates in the gold precipitation at arsenopyrite. Of course, real reaction mechanisms are much more complicated than Eqs. (3)–(5) and still need to be investigated.

Some facts apparently disagree with this approach; for instance, the samples leached in a ferric nitrate solution or polarized cathodically before gold deposition carry abundant surface products but show little affinity for gold uptake. This may be explained through the oxidized nature of surface alteration products that cannot transfer electrons to gold and that impede electron transfer to gold from the underlying arsenopyrite. On the other hand, one can notice a sympathetic correlation between the deposition of gold and the passivity of arsenopyrite surfaces. A similar parallel between passivation during anodic oxidation of galena and the quantity of metallic lead then deposited on the reacted surfaces at negative potentials was mentioned previously (Mikhlin et al., 2004a). The model of the disordered passive layer considers that the *n*-type conductivity and the potential fluctuations entail increased density of electrons at least on some surface spots, facilitating the reductive deposition of a metal. On the whole, both local chemical interactions and changes in the semiconducting properties of the mineral substrate seem to influence the reduction of gold ions, with their roles being presently underestimated.

4.3. Possibility of Coulomb blockade and its geochemical implication

Gold nanoparticles have attracted much interest in various fields of nanoscience, and their structure, physical and chemical properties have been extensively studied (Daniel and Astruc, 2004). Although the "invisible" gold largely consists of nanometer metallic particles, special characteristics potentially related with the small size have received very little attention in geochemistry and mineral processing (Hochella, 2002). The behavior of Au particles found in the current study is attributable to Coulomb blockade effects, which take place if the electrostatic energy, $E = e^2/2C$, is larger than the thermal energy kT (e is the fundamental charge unit, k is the Boltzmann's constant, and C stands for the particle capacitance). The effects were observed on gold nanoparticles about 2 nm or less at low temperatures in a majority of previous experimental studies. The I–V plots in Fig. 10 exhibit suppression of the tunneling currents and the conductance gap on gold nanoparticles but show a gradual rise in current with voltage rather than a Coulomb staircase. The presence of a large number of very small Au clusters invisible in STM (perhaps because they are weakly bonded to a substrate) cannot be excluded fully but looks unlikely. At the same time, the concurrence of the STS and XPS data for gold at arsenopyrite and other sulfide minerals (will be published elsewhere) confirms that the effect really takes place but is not an artifact. Accordingly, a question arises if and why the Coulomb blockade takes place on the particles as large as 20–30 nm in diameter at ambient temperatures.

To meet the requirement $e^2/2C > kT$, the particle capacitance C should be $<3.2 \times 10^{-18}$ F at 293 K, and the diameter d should be less than 20 nm, assuming, as a first approximation, that the gold clusters represent spherical capacitors ($C = 2\pi\varepsilon_0\varepsilon d$, $\varepsilon \approx 3$). The magnitude of the effect decreases in accordance with $1/d$ law as the particle size grows (Boyen et al., 2005). Real systems normally consist of two junctions, between the tip and a particle and a particle and the substrate, coupled in series (Amman et al., 1991; Tsuji et al., 2004). As a rule, possible leakage current from the second junction and electron trapping in the impurities in gold and in the environment of the particle impose stricter limitations on the particle size necessary to observe the single electron transitions. Han et al. (1998) have found, nevertheless, the Coulomb staircase behavior with gold particles of 12 nm supported on graphite at room temperature; the authors attributed this to the pure and uniform capped Au nanoparticles obtained under special conditions. In the current research, the gold particles were supported on the oxidized and disordered surfaces of arsenopyrite whose specific and still poorly understood properties are believed to determine passivation of the material and could impose a high impedance on the particle-support junction, favoring Coulomb blockade. A dielectric underlayer composed of elemental sulfur or other substances may form locally beneath the Au particle; in particular, Mycroft et al. (1995) observed a halo around an Au^0 particle on pyrite. On the other hand, the gold particle could be capped with an isolating layer of S^0 due to an interaction with HS^- or other sulfur species. Furthermore, a submonolayer of adsorbed sulfur may retard tunneling of electrons by modifying the electronic structure of the surface. It is noteworthy that Geng et al. (2005) have recently reported a suppression of electron hopping by H_2S within a system of Au nanoparticles as large as 13 nm.

One can anticipate that these effects will influence also electron transitions between a particle and redox agents situated in an aqueous phase or adsorbed on arsenopyrite and Au clusters. Usually, nanoscale particles possess enhanced reactivity; for example, a decrease in the particle size is thought to result in lowering the reduction potential, thus making the metal more susceptible towards oxidation (Pal, 2001). There are a series of studies in which Coulomb blockade was revealed in electrochemical reactions (see Daniel and Astruc, 2004 for a review). In particular, Chen and co-workers (see Chen, 2004 and references herein) discovered a quantized capacitance charging of gold nanoparticles protected with a monolayer of organic sulfides in aqueous electrolytes containing hydrophobic anions. Hence, Coulomb blockade or other mechanisms behind

the suppression of tunneling current should hinder both cathodic and anodic reactions on small particles, particularly the charge transfer steps of the growth and oxidative dissolution of gold. The limited rates both of precipitation and dissolution of nanoscale clusters may, therefore, in part control the deposition of "invisible" gold under hydrothermal conditions.

It is generally accepted in hydrometallurgy that the slow dissolution rates and low recoveries of "invisible" gold from refractory pyrite–arsenopyrite ores are due to gold either buried in accommodating minerals or products of their oxidation, or screened by a passive layer on the gold surface. The proposed mechanism predicts that the leaching of small metal particles could be impeded even if they are exposed to a lixiviant. An accelerating effect can be produced in this case by increasing the conductance of the surfaces in order to eliminate the Coulomb blockade. To understand the role of the electron transfer suppression in the deposition and the extraction of gold, we must know more about surfaces of the mineral substrate and metallic nanoparticles and their reactivity, including whether the ultrasmall Au particles really grow or/and dissolve slower than larger ones. Unfortunately, arsenopyrite surfaces have a rough topography, complicating SPM examination, and we plan to continue this work on pyrite.

5. Conclusions

Progressively increasing amounts of surface Fe(III)–O and As–O species, and S/Fe and S/As ratios in a non-stoichiometric layer of the sulfide phase have been determined for electrochemically oxidized arsenopyrite. The products formed in the sweep to a potential of the passivity region were shaped in about 100 nm protrusions of two sorts and then arranged in micrometer-size separate areas, but were largely mixed at higher potentials. The quantities of the substances were notably less after the ferric iron leaching in hydrochloric and sulfuric acid media. Passivity of arsenopyrite may be associated with the disordered, metal-deficient surface layer having moderate excess of sulfur rather than with the abundance of the oxidation products.

The treatment of arsenopyrite in 10^{-5}–10^{-3} M $HAuCl_4$ (pH 2) solutions resulted in the spontaneous deposition of 6–50 nm gold particles; only a minor share of gold was present as Au(I)–S species but its relative proportion increased as the total quantity of the surface gold fell. The electrochemical oxidation or aging of arsenopyrite in air promoted the following gold deposition; in contrast, the uptake of Au by the mineral preleached in the ferric chloride and sulfate solutions was about 10 times less as compared with fractured or polished samples. It may be concluded that reducing agents (As species, Fe^{2+}, etc.) formed as intermediates of arsenopyrite decomposition facilitate the Au^0 reduction and deposition and that the state of arsenopyrite surface plays a role as well.

STS showed a decrease in the tunneling current magnitudes with decreasing the Au particle size. This may be ascribed, together with the increase by 0.2–0.5 eV in the XPS Au 4f binding energies, to retarding the electron transitions by emerging electrostatic charge of a nanoparticle (Coulomb blockade). Probable mechanisms allowing the observation of Coulomb blockade effects on the relatively large particles at room temperature and their potential role in the deposition and hydrometallurgical recovery of "invisible" gold require further examination.

Acknowledgments

The authors thank Dr. C. Eggleston (Associated Editor), Dr. W. Barzyk and the anonymous referees for constructive reviews of this work and helpful suggestions to improve the original manuscript.

Associate editor: Carrick M. Eggleston

Appendix A. Supplementary data

Supplementary data associated with this article can be found, in the online version, at doi:10.1016/j.gca.2006.07.021.

References

Amman, M., Wilkins, R., Ben-Jacob, E., Maker, P.D., Jaklevic, R.C., 1991. Analytic solution for the current-voltage characteristic of two mesoscopic tunnel junctions coupled in series. *Phys. Rev. B* **43**, 1146–1149.

Barnes, H.L., 1979. *Geochemistry of Hydrothermal Ore Deposits*. Wiley, New York.

Barzyk, W., Kowal, A., Pomianowski, A., 2002. Noble metal (Ag, Au) cementation on non-stoichiometric cuprous sulphide grains. *Colloid Surf. A* **208**, 321–335.

Becker, U., Vaughan, D.J., Hochella Jr., M.F., 1997. The adsorption of gold to galena surfaces: calculation of adsorption/reduction energies, reaction mechanisms, XPS spectra, and STM images. *Geochim. Cosmochim. Acta* **61**, 3565–3585.

Becker, U., Rosso, K.M., Weaver, R., Warren, M., Hochella Jr., M.F., 2003. Metal island growth and dynamics on molybdenite surfaces. *Geochim. Cosmochim. Acta* **67**, 923–934.

den Besten, J., Jamieson, D.N., Ryan, C.G., 1999. Lattice location of gold in natural pyrite crystals. *Nucl. Instrum. Methods Phys. Res. B* **152**, 135–144.

Bou, C., Cruells, M., Romero, M.T., Viñals, J., 1998. Kinetics of the interaction of gold chloride solutions on arsenopyrite. *Hydrometallurgy* **48**, 303–360.

Boyen, H.-G., Ethirajan, A., Kästle, G., Weigl, F., Ziemann, P., Schmid, G., Garnier, M.G., Büttner, M., Oelhafen, P., 2005. Alloy formation of supported gold nanoparticles at their transition from clusters to solids: does size matter? *Phys. Rev. B* **94**, 016804.

Briggs, D., Seah, M.P., 1990. *Practical Surface Analysis. Vol. 1*, second ed. Wiley, New York.

Buckley, A.N., Woods, R., 1984. An X-ray photoelectron spectroscopic study of the oxidation of galena. *Appl. Surf. Sci.* **17**, 401–414.

Buckley, A.N., Hamilton, I.C., Woods, R., 1985. Investigation of the surface oxidation of sulfide minerals by linear potential sweep voltammetry and X-ray photoelectron spectroscopy. In: Forssberg, K.S.E. (Ed.), *Flotation of Sulfide Minerals*. Elsevier, Amsterdam, pp. 41–60.

Buckley, A.N., Walker, G.W., 1988–1989. The surface composition of arsenopyrite exposed to oxidizing environments. *Appl. Surf. Sci.* **35**, 227–240.

Bullen, H.A., Dorko, M.J., Oman, J.K., Garrett, S.J., 2003. Valence and core-level binding energy shifts in realgar (As_4S_4) and pararealgar (As_4S_4) arsenic sulfides. *Surf. Sci.* **531**, 319–328.

Cabri, L.J., Newville, M., Gordon, R.A., Crozier, E.D., Sutton, S.R., McMahon, G., Jiang, D.-T., 2000. Chemical speciation of gold in arsenopyrite. *Can. Mineral.* **38**, 1265–1281.

Cattarin, S., Flechter, S., Pettenkofer, C., Tributsch, H., 1990. Interfacial reactivity and oscillating behaviour of chalcopyrite cathodes during H_2O_2 reduction II. Characterization of electrode corrosion. *J. Electrochem. Soc.* **137**, 3484–3492.

Chen, S., 2004. Chemical manipulations of nanoscale electron transfers. *J. Electroanal. Chem.* **574**, 153–165.

Costa, M.C., Botelho do Rego, A.M., Abrantes, L.M., 2002. Characterization of a natural and an electro-oxidized arsenopyrite: a study on electrochemical and X-ray photoelectron spectroscopy. *Int. J. Miner. Process.* **65**, 83–108.

Cruz, R., Lázaro, I., Rodríguez, J.M., Monroy, M., González, I., 1997. Surface characterization of arsenopyrite in acidic medium by triangular scan voltammetry on carbon paste electrodes. *Hydrometallurgy* **46**, 303–319.

Daniel, M.-C., Astruc, D., 2004. Gold nanoparticles: assembly, supramolecular chemistry, quantum size-related properties, and applications toward biology, catalysis, and nanotechnology. *Chem. Rev.* **104**, 293–346.

Eggleston, C.M., Hochella Jr., M.F., 1991. Scanning tunneling microscopy of galena surface oxidation and sorption of aqueous gold. *Science* **254**, 983–986.

Eggleston, C.M., Hochella Jr., M.F., 1993. Tunneling spectroscopy applied to PbS (1 0 0) surfaces: fresh surfaces, oxidation and sorption of aqueous gold. *Am. Mineral.* **78**, 877–883.

Eyert, V., Höck, K.-H., Fiechter, S., Tributsch, H., 1998. Electronic structure of FeS_2: the crucial role of electron–lattice interaction. *Phys. Rev. B* **57**, 6350–6359.

Geng, J., Thomas, M.D.R., Shephard, D.S., Johnson, B.F.G., 2005. Suppressed electron hopping in a Au nanoparticle/H_2S system: development towards a H_2S nanosensor. *Chem. Commun.* **14**, 1895–1897.

Genkin, A.D., Bortnikov, N.S., Cabri, L.J., Wagner, F.E., Stanley, C.J., Safonov, Y.G., McMahon, G., Friedl, J., Kerzin, A.L., Gamyanin, G.N., 1998. A multidisciplinary study of invisible gold in arsenopyrite from four mesothermal gold deposits in Siberia, Russian Federation. *Econ. Geol.* **93**, 463–487.

Gheorghiu-de La Rocque, A.D., Belin-Ferré, E., Fontaine, M.-F., Adriaenssens, G.J., 2002. XPS studies of Cu incorporation in arsenic chalcogenides. *J. Non-Cryst. Solids* **299–302**, 953–957.

Fleet, M.E., Mumin, A.H., 1997. Gold-bearing arsenian pyrite and marcasite and arsenopyrite from Carlin Trend gold deposits and laboratory synthesis. *Am. Mineral.* **82**, 182–193.

Hackl, R.P., Dreisinger, D.B., Peters, E., King, J.A., 1995. Passivation of chalcopyrite during oxidative leaching in sulfate media. *Hydrometallurgy* **39**, 25–48.

Heasman, D.M., Sherman, D.M., Ragnarsdottir, K.V., 2003. The reduction of aqueous Au^{3+} by sulfide minerals and green rust phases. *Am. Mineral.* **88**, 725–738.

Han, M.Y., Zhou, L., Quek, C.H., Li, S.F.Y., Huang, W., 1998. Room temperature Coulomb staircase on pure and uniform surface-capped gold nanoparticles. *Chem. Phys. Lett.* **287**, 47–52.

Hochella Jr., M.F., 2002. There's plenty of room at the bottom: nanoscience in geochemistry. *Geochim. Cosmochim. Acta* **66**, 735–743.

Hövel, H., Grimm, B., Pollmann, M., Reihl, B., 1998. Cluster-substrate interaction on a femtosecond time scale revealed by a high-resolution photoemission study of the Fermi-level onset. *Phys. Rev. Lett.* **81**, 4608–4611.

Hyland, M.M., Bancroft, G.M., 1989. An XPS study of gold deposition at low temperatures on sulphide minerals: reducing agents. *Geochim. Cosmochim. Acta* **53**, 367–372.

Jean, G.E., Bancroft, G.M., 1985. An XPS and SEM study of gold deposition at low temperatures on sulphide mineral surfaces: concentration of gold by adsorption/reduction. *Geochim. Cosmochim. Acta* **49**, 979–987.

Jones, R.A., Koval, S.F., Nesbitt, H.W., 2003. Surface alteration of arsenopyrite (FeAsS) by *Thiobacillus ferrooxidans*. *Geochim. Cosmochim. Acta* **67**, 955–965.

Kartio, I., Wittstock, G., Laajalehto, K., Hirsch, D., Simola, J., Laiho, T., Szargan, R., Suoninen, E., 1997. Detection of elemental sulphur on galena oxidized in acidic solutions. *Int. J. Miner. Process.* **51**, 293–301.

Kiss, L., 1988. *Kinetics of Electrochemical Metal Dissolution*. Akadémiai Kiadó, Budapest.

Kostina, G.M., Chernyak, A.S., 1976. Electrochemical conditions for the oxidation of pyrite and arsenopyrite in alkaline and acid solutions. *Zh. Prikl. Khim.* **49**, 1534–1540.

Lázaro, I., Cruz, R., González, I., Monroy, M., 1997. Electrochemical oxidation of arsenopyrite in acidic media. *Int. J. Miner. Process.* **50**, 63–75.

Lin, H.K., Zheng, Z.M., 1997. Electrochemical oxidation of arsenopyrite in chloride solutions. *Hydrometallurgy* **42**, 411–424.

Maddox, L.M., Bancroft, G.M., Scaini, M.J., Lorimer, J.W., 1998. Invisible gold: comparison of Au deposition on pyrite and arsenopyrite. *Am. Mineral.* **83**, 1240–1245.

McGuire, M.M., Banfield, J.F., Hamers, R.J., 2001a. Quantitative determination of elemental sulfur at the arsenopyrite surface after oxidation by ferric iron: mechanistic implications. *Geochem. Trans.* **4**, 23–27.

McGuire, M.M., Edwards, K.J., Banfield, J.F., Hamers, R.J., 2001b. Kinetics, surface chemistry, and structural evolution of microbially mediated sulfide mineral dissolution. *Geochim. Cosmochim. Acta* **65**, 1243–1258.

McGuire, M.M., Jallad, K.N., Ben-Amotz, D., Hamers, R.J., 2001c. Chemical mapping of elemental sulfur on pyrite and arsenopyrite surfaces using near-infrared Raman imaging spectroscopy. *Appl. Surf. Sci.* **178**, 105–115.

Mikhlin, Yu.L., Kuklinskii, A.V., Pashkov, G.L., Asanov, I.P., 2001. Pyrrhotite electrooxidation in acid solutions. *Russ. J. Electrochem.* **37**, 1277–1282.

Mikhlin, Yu.L., Kuklinskiy, A.V., Pavlenko, N.I., Varnek, V.A., Asanov, I.P., Okotrub, A.V., Selyutin, G.E., Solovyev, L.A., 2002. Spectroscopic and XRD studies of the air degradation of acid-reacted pyrrhotites. *Geochim. Cosmochim. Acta* **66**, 4077–4087.

Mikhlin, Y., Shipin, D., Kuklinskiy, A., Asanov, I., 2003a. Electrochemical reactions of arsenopyrite in acidic solutions. In: Doyle, F.M., Kelsall, G.H., Woods, R. (Eds.), *Electrochemistry in Mineral and Metal Processing VI*. The Electrochemical Soc. Proceedings, vol. 2003-18. Pennington, NJ, pp. 120–130.

Mikhlin, Y., Tomashevich, Y., Kuklinskiy, A., Shipin, D., Asanov, I., Okotrub, A., Varnek, V., Bausk, N., 2003b. Passivation of sulfide minerals: are the metal-deficient layers responsible? In: Doyle, F.M., Kelsall, G.H., Woods, R. (Eds.), *Electrochemistry in Mineral and Metal Processing VI*. The Electrochemical Soc. Proceedings, vol. 2003-18. Pennington, NJ, pp. 96–107.

Mikhlin, Yu., Kuklinskiy, A., Mikhlina, E., Kargin, V., Asanov, I., 2004a. Electrochemical behaviour of galena (PbS) in aqueous nitric acid and perchloric acid solutions. *J. Appl. Electrochem.* **34**, 37–46.

Mikhlin, Yu.L., Tomashevich, Ye.V., Asanov, I.P., Okotrub, A.V., Varnek, V.A., Vyalikh, D.V., 2004b. Spectroscopic and electrochemical characterization of the surface layers of chalcopyrite ($CuFeS_2$) reacted in acidic solutions. *Appl. Surf. Sci.* **225**, 395–409.

Mikhlin, Yu., Tomashevich, Ye., 2005. Pristine and reacted surfaces of pyrrhotite and arsenopyrite as studied by X-ray absorption near-edge structure spectroscopy. *Phys. Chem. Miner.* **32**, 19–27.

Mott, N.F., Davis, E.A., 1979. *Electron Processes in Non-crystalline Materials*. Clarendon Press, Oxford.

Mycroft, J.R., Bancroft, G.M., McIntyre, N.S., Lorimer, J.W., 1995. Spontaneous deposition of gold on pyrite from solution containing Au(III) and Au(I) chlorides: Part I, a surface study. *Geochim. Cosmochim. Acta* **59**, 3351–3365.

Nesbitt, H.W., Muir, I.J., Pratt, A.R., 1995. Oxidation of arsenopyrite by air and air-saturated, distilled water, and implications for mechanism of oxidation. *Geochim. Cosmochim. Acta* **59**, 1773–1786.

Ohgi, T., Fujita, D., 2003. Single electron charging effects in gold nanoclusters on alkanedithiol layers with different molecular lengths. *Surf. Sci.*, 294–299.

O'Loughlin, E.J., Kelly, S.D., Kemner, K.M., Csencsits, R., Cook, R.E., 2003. Reduction of Ag^{I}, Au^{III}, Cu^{II}, and Hg^{II} by Fe^{II}/Fe^{III} hydroxysulfate green rust. *Chemosphere* **53**, 437–446.

Pal, A., 2001. Photochemical dissolution of gold nanoparticles by bromine containing trihalomethanes (THMs) in an aqueous triton X-100 medium and its analytical application. *J. Photochem. Photobiol. A* **142**, 59–65.

Palenik, C.S., Utsunomiya, S., Reich, M., Kesler, S.E., Wang, L., Ewing, R.C., 2004. "Invisible" gold revealed: direct imaging of gold nanoparticles in a Carlin-type deposit. *Am. Mineral.* **89**, 1359–1366.

Paktunc, D., Foster, A., Heald, S., Laflamme, G., 2003. Speciation and characterization of arsenic in gold ores and cyanidation tailings using X-ray absorption spectroscopy. *Geochim. Cosmochim. Acta* **68**, 969–983.

Pratt, A.R., Nesbitt, H.W., 2000. Core level electron binding energies of realgar (As_4S_4). *Am. Mineral.* **85**, 619–622.

Reich, M., Kesler, S.E., Utsunomiya, S., Palenik, C.S., Chryssoulis, S.L., Ewing, R.C., 2005. Solubility of gold in arsenian pyrite. *Geochim. Cosmochim. Acta* **69**, 2781–2796.

Rimstidt, J.D., Vaughan, D.J., 2003. Pyrite oxidation: a state-of-the-art assessment of the reaction mechanism. *Geochim. Cosmochim. Acta* **67**, 873–880.

Richardson, S., Vaughan, D.J., 1989. Arsenopyrite: a spectroscopic investigation of altered surfaces. *Mineral. Mag.* **53**, 223–229.

Sakharova, M.S., Batrakova, Yu.A., Ryakhovskaya, S.K., 1975. Investigation of electrochemical interactions between sulphides and bearing-solutions. *Trans. Geokhimiya* **5**, 740–745.

Scaini, M.J., Bancroft, G.M., Knipe, S.W., 1997. An XPS, AES, and SEM study of the interactions of gold and silver chloride species with PbS and FeS_2: comparison to natural samples. *Geochim. Cosmochim. Acta* **61**, 1223–1231.

Scaini, M.J., Bancroft, G.M., Knipe, S.W., 1998. Reactions of aqueous Au^{1+} sulfide species with pyrite as a function of pH and temperature. *Am. Mineral.* **83**, 316–322.

Schaufuss, A.G., Nesbitt, H.W., Scaini, M.J., Hoechst, H., Bancroft, M.G., Szargan, R., 2000. Reactivity of surface sites on fractured arsenopyrite (FeAsS) toward oxygen. *Am. Mineral.* **85**, 1754–1766.

Simon, G., Huang, H., Penner-Hahn, J.E., Kesler, S.E., Kao, L.-S., 1999. Oxidation state of gold and arsenic in gold-bearing arsenian pyrite. *Am. Mineral.* **84**, 1071–1079.

Tauson, V.L., 1999. Gold solubility in the common gold-bearing minerals: experimental evaluation and application to pyrite. *Eur. J. Miner.* **11**, 937–947.

Tossell, J.A., Vaughan, D.J., Burdett, J.K., 1981. Pyrite, marcasite, and arsenopyrite type minerals: crystal chemical and structural principles. *Phys. Chem. Miner.* **7**, 177–184.

Tsendin, K.D. (Ed.), 1996. *Electron Phenomena in Chalcogenide Glassy Semiconductors*. Nauka, St. Peterburg.

, H., Arai, N., Matsumoto, T., Ueno, K., Gotoh, Y., Adachi, K., Kotaki, H., Ishikawa, J., 2004. Silver nanoparticle formation in thin oxide layer on silicon by silver-negative-ion implantation for Coulomb blockade at room temperature. *Appl. Surf. Sci.* **238**, 132–137.

Yunmei, Y., Yongxuan, Z., Williams-Jones, A.E., Zhenmin, G., Dexian, L., 2004. A kinetic study of the oxidation of arsenopyrite in acidic solutions: implications for the environment. *Appl. Geochem.* **19**, 435–444.

Widler, A.M., Seward, T.M., 2002. The adsorption of gold(I) hydrosulphide complexes by iron sulphide surfaces. *Geochim. Cosmochim. Acta* **66**, 383–402.